Radioiodinated Flavones for in Vivo Imaging of β-Amyloid Plaques in the Brain

Masahiro Ono,*,† Naoko Yoshida,† Kenichi Ishibashi,‡ Mamoru Haratake,† Yasushi Arano,§ Hiroshi Mori,‡ and Morio Nakayama†

Department of Hygienic Chemistry, Graduate School of Biomedical Sciences, Nagasaki University, 1-14 Bunkyo-machi, Nagasaki 852-8521, Japan, Department of Neuroscience, Osaka City University Medical School, 1-4-3 Asahi-machi, Abeno-ku, Osaka 545-8585, Japan, Department of Molecular Imaging and Radiotherapy, Graduate School of Pharmaceutical Sciences, Chiba University, 1-8-1 Inohana, Chuo-ku, Chiba 260-8675, Japan

Received July 4, 2005

In vivo imaging of β-amyloid (Aβ) peptide aggregates in the brain may lead to early detection of Alzheimer's disease (AD) and monitoring of the progression and effectiveness of AD treatment. The purpose of this study was to develop novel amyloid imaging agents based on flavone as a core structure. Radioiodinated flavone derivatives were designed and synthesized. The binding affinities of flavone derivatives for Aβ aggregates varied from 13 to 77 nM. When in vitro plaque labeling was carried out using post-mortem AD brain sections, all flavones intensely stained not only amyloid plaques but also cerebrovascular amyloids. In biodistribution studies using normal mice, they displayed high brain uptakes ranging from 3.2 to 4.1% ID/g at 2 min postinjection. The radioactivity washed out from the brain rapidly (0.5−1.9% ID/g at 30 min), which is highly desirable for amyloid imaging agents. The results in the study suggest that these classes of radioiodinated flavones may be useful candidates as potential imaging agents for amyloid plaques.

Introduction

Alzheimer's disease (AD) is a progressive neurodegenerative disorder characterized by abundant senile plaques (SPs) composed of β-amyloid (Aβ) peptides and numerous neurofibrillary tangles (NFTs) formed by filaments of highly phosphorylated τ proteins in the brain.[1] Currently, the definitive confirmation of AD is dependent on only post-mortem histopathological examination of SPs and/or NFTs in the brain. Therefore, in vivo imaging of amyloid plaques in the living brain may be useful for early detection of AD or monitoring of the progression and effectiveness of novel treatments that are currently being investigated.[2−4]

Extensive research has been undertaken to develop radiolabeled amyloid-specific imaging agents by several research groups (Figure 1). Several agents including [^{11}C]-4-*N*-methylamino-4′-hydroxystilbene ([^{11}C]SB-13),[5] [^{11}C]-2-(4-(methylamino)phenyl)-6-hydroxybenzothiazole ([^{11}C]-6-OH-BTA-1),[6] and [^{18}F]-2-(1-(2-(*N*-(2-fluoroethyl)-*N*-methylamino)naphthalene-6-yl)ethylidene)malononitrile ([^{18}F]FDDNP)[7] have been reported for positron emission tomography (PET) imaging of amyloid plaques in AD patients. Encouraging results reported with these agents in AD patients suggest that the development of imaging agents for detecting amyloid plaques in the living human brain is possible.[8−10] It is well-known that PET provides better functional information with higher resolution and sensitivity than single photon emission computed tomography (SPECT). However, since SPECT imaging is more practical as a routine clinical diagnostic procedure, the development of amyloid imaging agents for SPECT has been highly anticipated. In an attempt to develop ^{123}I tracers for SPECT imaging, many radioiodinated probes based on various core structures have been studied. Among the radioiodinated ligands evaluated, 6-iodo-2-(4′-dimethylamino)phenylimidazo[1,2-a]-pyridine (IMPY) (Figure 1) has been characterized as a potential SPECT imaging agent for amyloid plaques.[11,12] IMPY displayed selective amyloid plaque labeling in ex vivo autoradiography using double transgenic mice (PSAPP) as a model of AD.[13] In addition, 2-(3′-iodo-4′-aminophenyl)-6-hydroxybenzothiazole (6-OH-BTA-O-3′-I) (Figure 1) also showed desirable in vitro and in vivo properties.[14] However, no SPECT imaging agents have been evaluated in humans until now.

Recently, the effects of polyhydroxyflavones on the formation, extension, and destabilization of Aβ aggregates were studied in vitro.[15] These flavones dose-dependently inhibited the formation of Aβ aggregates, as well as destabilizing preformed Aβ aggregates, indicating that they could directly interact with Aβ aggregates. The findings in this previous report prompted us to apply flavones as a novel core structure of amyloid imaging agents. Furthermore, some recent studies have shown that electron-donating groups such as methylamino, dimethylamino, methoxy, and hydroxy groups play a critical role in the binding affinity to Aβ aggregates.[5,6,12,16−19] With these considerations in mind, we designed four radioiodinated flavones with a radioiodine at the 6 position and an electron-donating group at the 4′ position (Figure 2).

In the present study, we synthesized a series of flavone derivatives and evaluated their usefulness as in vivo amyloid imaging agents. To our knowledge, this is the first time flavones have been proposed as amyloid imaging agents for detecting AD.

* To whom correspondence should be addressed. Phone: 81-95-819-2443. Fax: 81-95-819-2442. E-mail: mono@net.nagasaki-u.ac.jp.
† Nagasaki University.
‡ Osaka City University Medical School.
§ Chiba University.

10.1021/jm050635e CCC: $30.25
Published on Web 10/19/2005

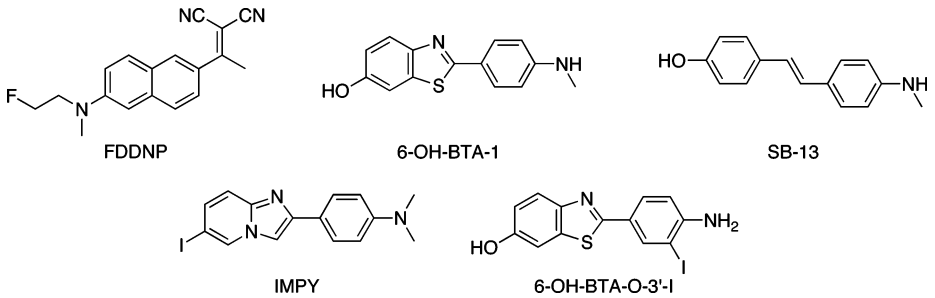

Figure 1. Chemical structures of amyloid imaging agents previously reported.

Scheme 1

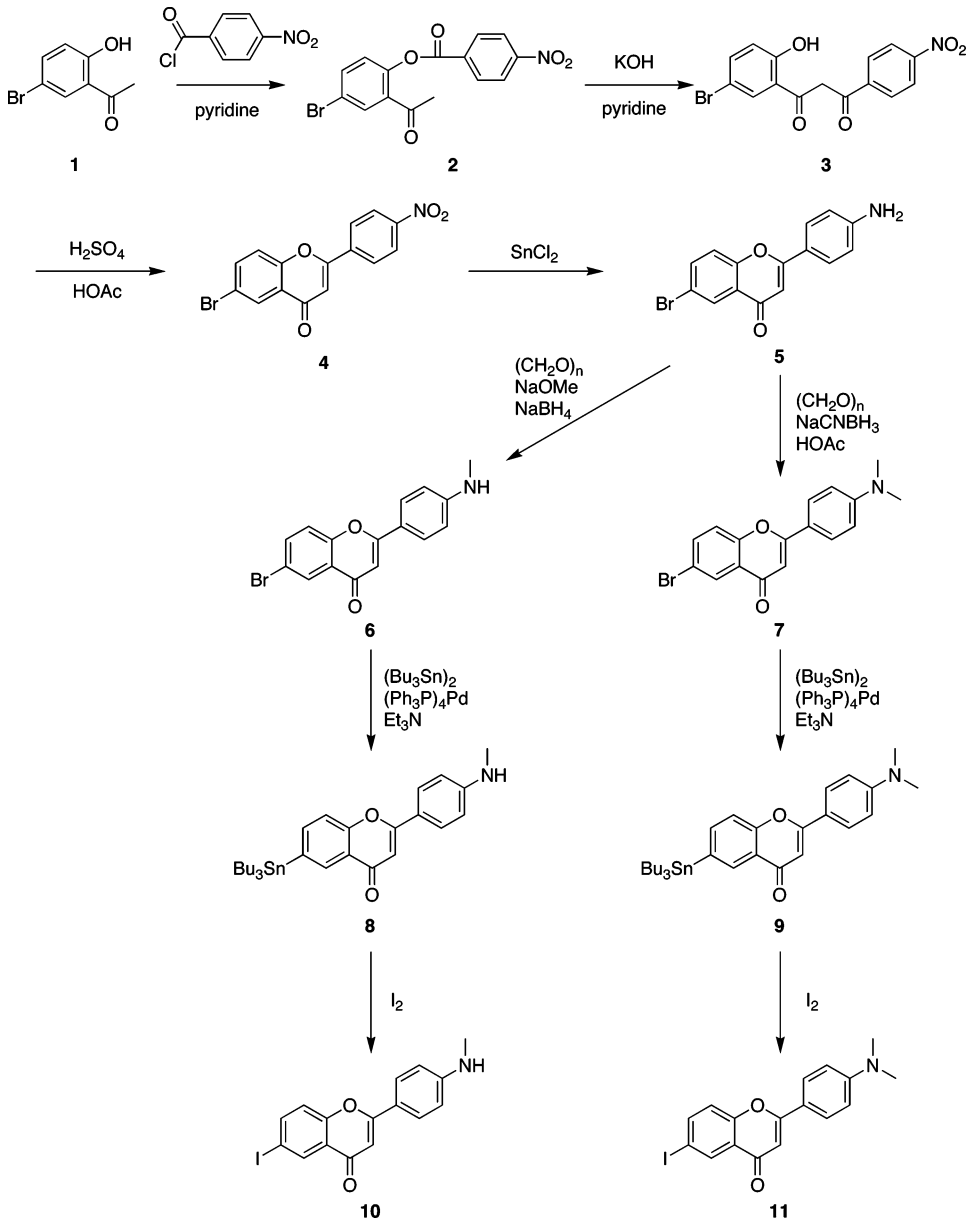

Results and Discussion

Chemistry. The most common method of synthesizing flavones is known as the Baker−Venkataraman transformation.[20] Schemes 1 and 2 illustrate an application of the conventional Baker−Venkataraman synthesis. In this process, a hydroxyacetophenone (**1**, **12**) is first converted into a benzoyl ester (**2**, **13**), and this species is then treated with a base, forming a 1,3-diketone (**3**, **14**). Treatment of this diketone with acid leads to generation of the desired flavone (**4**, **15**). The free amino derivative **5** was readily prepared from **4** by reduction with $SnCl_2$ (84% yield). Conversion of **5** to the monomethylamino derivative **6** was achieved by a method previously reported[21] (39% yield). Compound **5** was also converted to the dimethylamino derivative **7** by an efficient method[5,19] with paraformaldehyde, sodium cyanoborohydride, and acetic acid (86% yield). Compound **15** was converted to **16** by demethylation

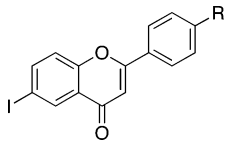

Figure 2. Chemical structure of radioiodinated flavone derivatives. Compounds reported here include the following: R = NHMe (**10**), NMe_2 (**11**), OMe (**19**), OH (**20**).

with BBr_3 in CH_2Cl_2 (13% yield). The tributyltin derivatives (**8**, **9**, **17**, and **18**) were prepared from the corresponding bromo compounds (**6**, **7**, **15**, and **16**) using a bromo to tributyltin exchange reaction catalyzed by Pd(0) for yields of 37%, 17%, 69%, and 43%, respectively. The tributyltin derivatives (**8**, **9**, and **17**) were readily reacted with iodine in chloroform at room temperature to give the iodo derivatives, compounds **10**, **11**, and **19** at yields of 29%, 47%, and 72%, respectively. Compound **20** was obtained in 44% yield from **19** by the same reaction to prepare **16**. Furthermore, these tributyltin derivatives (**8**, **9**, **17**, and **18**) can be also used as the starting materials for radioiodination in preparation of [^{125}I]**10**, [^{125}I]**11**, [^{125}I]**19**, and [^{125}I]**20**. Novel radioiodinated flavones were achieved by an iododestannylation reaction using hydrogen peroxide as the oxidant, which produced the desired radioiodinated ligands (Scheme 3). It was anticipated that the no-carrier-added preparation would result in a final product bearing a theoretical specific activity similar to that of ^{125}I (2200 Ci/mmol). The radiochemical identities of the radioiodinated ligands were verified by co-injection with nonradioactive compounds by their HPLC profiles. The final radioiodinated compounds [^{125}I]**10**, [^{125}I]**11**, [^{125}I]**19**, and [^{125}I]**20** showed a single radioactivity peak at retention times of 9.3, 19.9, 13.7, and 4.2 min, respectively, identical to those of nonradioactive compounds **10**, **11**, **19**, and **20** (Table 1). Four radioiodinated products were obtained in 55−70% radiochemical yields with radiochemical purities of >95% after purification by HPLC.

Binding Studies Using A*β* Aggregates in Solution. The binding studies of [^{125}I]**11** to aggregates of Aβ(1−40) and Aβ(1−42) were carried out. Transformation of the saturation binding of [^{125}I]**11** to Scatchard plots

Scheme 2

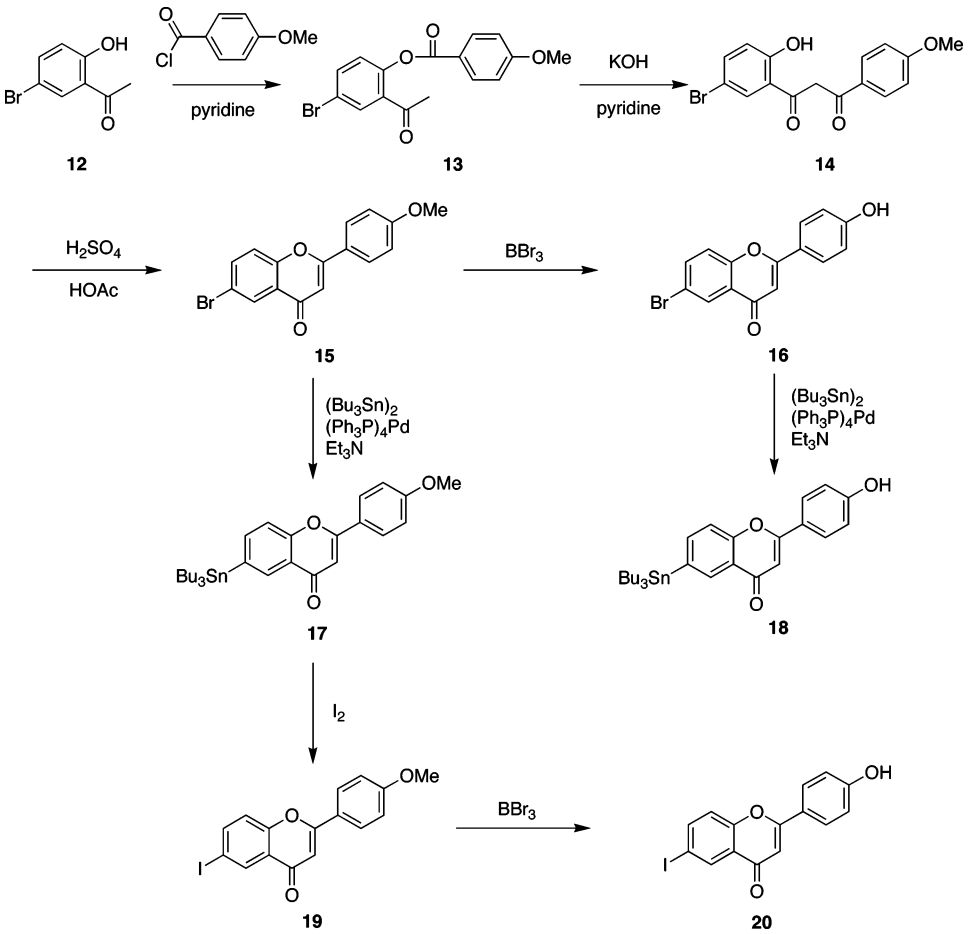

Scheme 3

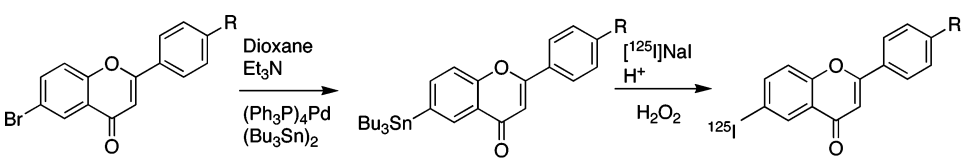

R: NHMe (**10**), NMe_2 (**11**), OMe (**19**), OH (**20**)

Table 1. HPLC Data and Partition Coefficients for [^{125}I]**10**, [^{125}I]**11**, [^{125}I]**19**, and [^{125}I]**20**

compd	retention time (min)[a]	log PC[b]
[^{125}I]**10**	9.3	2.15(0.01)
[^{125}I]**11**	19.9	2.69(0.01)
[^{125}I]**19**	13.7	2.41(0.03)
[^{125}I]**20**	4.2	1.92(0.01)

[a] Using a mixture of H_2O/acetonitrile (2/3) as the mobile phase. [b] Octanol/buffer (0.1 M phosphate buffered saline, pH 7.4) partition coefficients. Each value represents the mean (SD in parentheses) of three experiments.

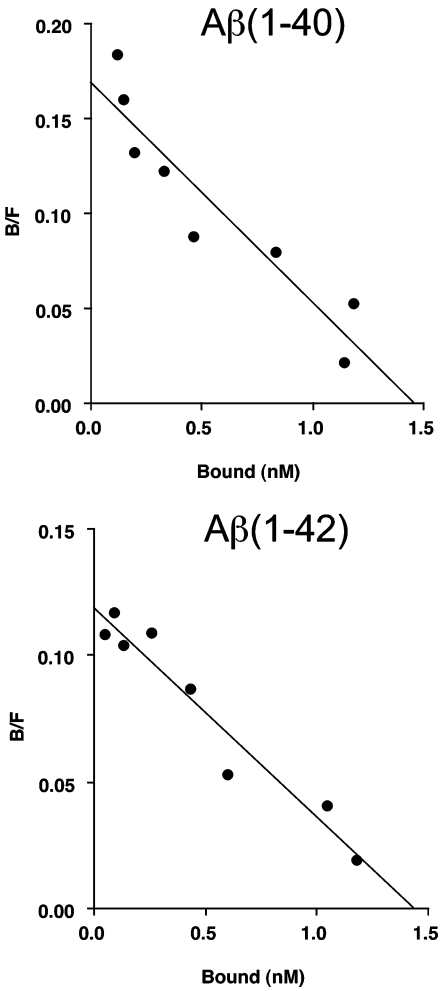

Figure 3. Scatchard plots of [^{125}I]**11** binding to aggregates of Aβ(1−40) and Aβ(1−42). [^{125}I]**11** displayed one-site binding. High-affinity binding with K_d values in a nanomolar range was obtained (K_d = 12.3 and 17.6 nM for Aβ(1−40) and Aβ(1−42) aggregates, respectively).

gave linear plots, suggesting one binding site. [^{125}I]**11** showed excellent binding affinity for both Aβ(1−40) (K_d = 12.4 ± 2.3 nM) and Aβ(1−42) (K_d = 17.4 ± 5.7 nM) aggregates (Figure 3). Binding affinities of nonradioactive flavone derivatives (compound **10**, **11**, **19**, and **20**) were evaluated with inhibition studies against [^{125}I]**11** binding on Aβ(1−40) and Aβ(1−42) aggregates. As shown in Table 2, all flavone derivatives competed well with [^{125}I]**11** binding on Aβ(1−40) and Aβ(1−42) aggregates. The K_i values estimated for **10**, **11**, **19**, and **20** were 23, 13, 29, and 73 nM for Aβ(1−40) aggregates and 30, 16, 38, and 77 nM for Aβ(1−42) aggregates, respectively. These K_i values suggested that the new series of flavones had high binding affinity for Aβ(1−40) and Aβ(1−42) aggregates in the following order: **11** > **10** > **19** > **20**. No marked difference between Aβ(1−40) and Aβ(1−42) aggregates was observed in their K_i values. It is especially noteworthy that compounds **10**, **11**, **19**, and **20** could bind not only Aβ(1−40) aggregates but also Aβ(1−42) aggregates, as we aim to develop novel probes that can detect diffuse plaques mainly composed of Aβ(1−42). More interestingly, when thioflavin T and Congo Red were evaluated for their competition against [^{125}I]**11** binding on Aβ(1−40) and Aβ(1−42) aggregates, high K_i values (> 1000 nM) were observed (Table 2), indicating poor binding competition. This finding suggests that these flavones may have a binding site on Aβ aggregates different from that of thioflavin T and Congo Red, although additional studies regarding the selectivity of binding affinity for Aβ aggregates are required.

Table 2. Inhibition Constants of Compounds on Ligand Binding to Aggregates of Aβ(1−40) and Aβ(1−42)

	K_i (nM)	
compd	Aβ(1−40)	Aβ(1−42)
10	22.6 ± 3.4	30.0 ± 3.4
11	13.2 ± 0.2	15.6 ± 2.4
19	29.0 ± 3.2	38.3 ± 8.1
20	72.5 ± 8.2	77.2 ± 9.2
thioflavin T	>1000	>1000
Congo Red	>1000	>1000

Neuropathological Staining on AD Brain Sections. Since the in vitro binding assays demonstrated the high binding affinity of the flavone derivatives for Aβ(1−40) and Aβ(1−42) aggregates (Table 2), compounds **10**, **11**, **19**, and **20** were investigated for their neuropathological staining of amyloid plaques and NFTs in human AD brain sections (Figure 4). Compounds **10**, **11**, **19**, and **20** intensely stained amyloid plaques (Figure 4A,E,I,M), neuritic plaques (Figure 4B,F,J,N), and cerebrovascular amyloids (Figure 4C,G,K,O) with nearly the same staining pattern. However, as seen in Figure 4A,E,I,M, these flavone compounds did not intensely stain the core region in so-called classical amyloid plaques, unlike the thioflavin T and Congo Red derivatives previously reported as amyloid imaging probes, indicating that flavone derivatives may have somewhat distinct binding characteristics for amyloid fibrils. The binding characteristics of the flavone derivatives for amyloid plaques in human AD sections may be relevant to the phenomenon observed in the in vitro binding assay; they may occupy a binding site on Aβ aggregates different from that of thioflavin T and Congo Red. Such a binding characteristic of the present flavone derivatives is thought to be related to the recent finding that a similar compound with a flavone backbone structure has a binding affinity with amyloid fibrils and the APP sequence.[22] However, this issue regarding the binding property of the flavone derivatives remains unresolved. These flavone derivatives appeared to stain not only neuritic amyloid plaques but also diffuse amyloid plaques, which are known to be mainly composed of Aβ(1−42)[23] and to be the initial pathological change of AD.[24] Thus, flavone derivatives with high binding affinity for Aβ-(1−42)-positive diffuse plaques may be more useful for presymptomatic detection of AD pathology. Furthermore, compounds **10**, **11**, **19**, and **20** also showed high binding affinity for NFTs in the AD sections (Figure 4D,H,L,P). A previous study reported that a remarkable

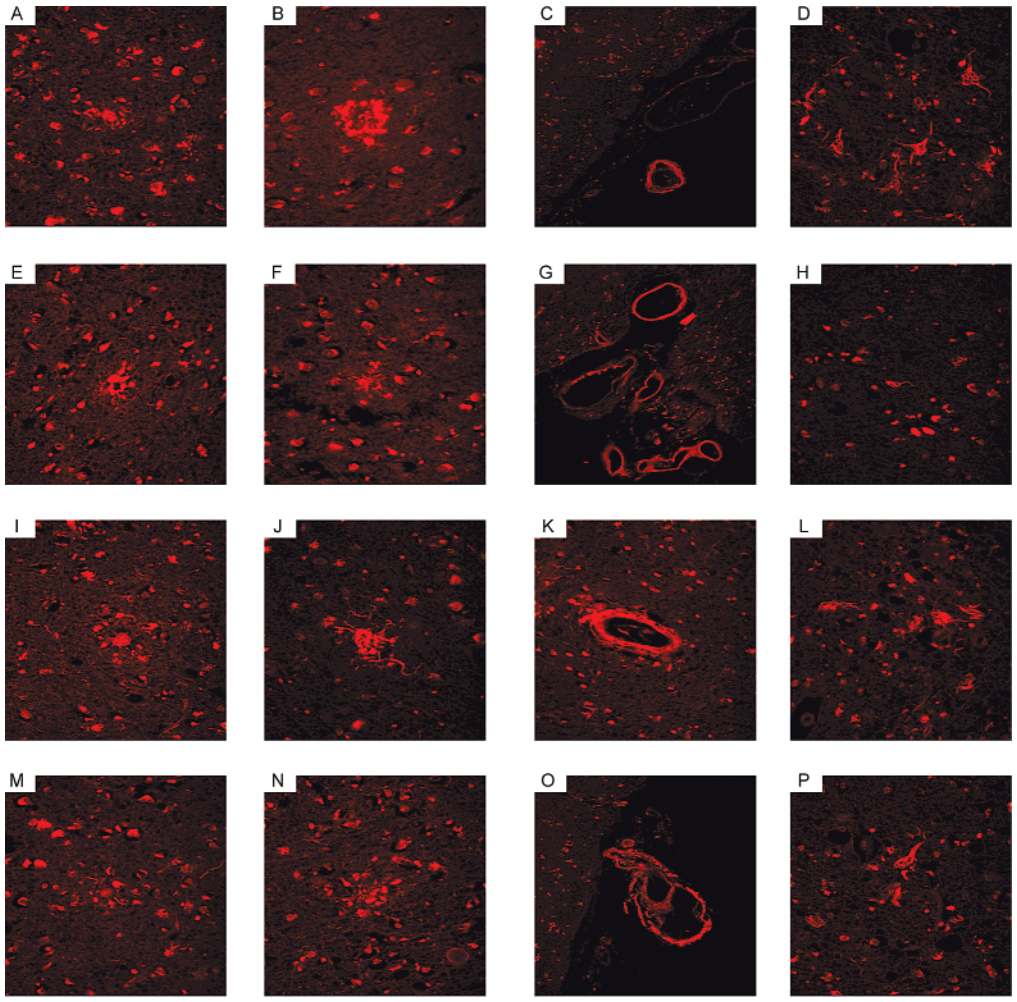

Figure 4. Neuropathological staining of compounds **10** (A−D), **11** (E−H), **19** (I−L), and **20** (M−P) on 5 μm AD brain sections from the temporal cortex. Amyloid plaques (A, E, I, M) are clearly stained with compounds **10**, **11**, **19**, and **20** (40× magnification). Clear staining of neuritic plaques (B, F, J, N) and cerebrovascular amyloid (C, G, K, O) was also obtained. Many NFTs (D, H, L, P) are intensely stained with compounds **10**, **11**, **19**, and **20** (40× magnification).

accumulation of NFTs in the hippocampus and entorhinal cortex has been observed at an early stage of AD.[25] Since flavone derivatives can strongly bind NFTs, they would detect an increase of NFT accumulation in the hippocampus and entorhinal cortex of the AD brain. These findings suggested that the flavone derivatives **10**, **11**, **19**, and **20** can bind amyloid fibrils and NFTs without the backbone structure of thioflavin T or Congo Red and that quantitative evaluation of their cerebral localization may provide useful information on Aβ and τ pathology.

Biodistribution Studies. Four radioiodinated flavone ligands ([^{125}I]**10**, [^{125}I]**11**, [^{125}I]**19**, and [^{125}I]**20**) were evaluated for their in vivo biodistribution in normal mice. A biodistribution study provides critical information on brain penetration. Generally, a freely diffusible compound with an optimal log PC value of 2−3 will have an initial brain uptake of 2−3% dose/whole brain at 2 min after iv injection.[26] All four ligands examined in this study displayed optimal lipophilicities as reflected by their log PC values of 1.94, 2.69, 2.41, and 1.92 for [^{125}I]-**10**, [^{125}I]**11**, [^{125}I]**19**, and [^{125}I]**20**, respectively (Table 1). As expected, these ligands displayed high brain uptakes ranging from 3.2 to 4.1% ID/g brain at 2 min postinjection, indicating a level sufficient for brain imaging probes (Table 3). In addition, they displayed good clearance from the normal brain with 1.2, 1.0, 0.17, and 0.08% ID/g at 60 min postinjection for [^{125}I]**10**, [^{125}I]**11**, [^{125}I]**19**, and [^{125}I]**20**, respectively (Table 3). These values were equal to 29%, 27%, 4.3%, and 2.4% of initial brain uptake peak for [^{125}I]**10**, [^{125}I]**11**, [^{125}I]**19**, and [^{125}I]**20**, respectively. Since the normal brain has no Aβ plaques to trap the agent, the washout from the normal brain should be fast. These desirable pharmacokinetics demonstrated by radioiodinated flanones are critical to obtain a higher signal-to-noise ratio earlier in the AD brain. Radioiodinated amyloid imaging agents such as [^{125}I]TZDM,[16] [^{125}I]IBOX,[17] [^{125}I]*m*-I-stilbene,[18] and [^{125}I]-benzofuran[19] reported previously showed high brain uptakes, but the washout rates from the normal brain were relatively slow. The slow washout rate from the brain leads to a high background activity and prevents the visualization of amyloid plaques in the AD brain. Currently, few reports describing radioiodinated amyloid agents with both high initial brain uptake and rapid washout from the normal brain have been available except for IMPY[11−13] and 6-OH-BTA-O-3′-I.[14] The appropriate in vivo properties observed for radioiodinated flavones in the present study (higher brain uptake and faster washout from the normal brain) make them useful candidates as SPECT tracers for amyloid imaging.

Table 3. Biodistribution of Radioactivity after Intravenous Administration of [^{125}I]**10**, [^{125}I]**11**, [^{125}I]**19**, and [^{125}I]**20** in Mice

	biodistribution of radioactivity[a] for time after injection			
tissue	2 min	10 min	30 min	60 min
		[^{125}I]**10**		
blood	1.89(0.28)	1.39(0.10)	1.34(0.07)	1.50(0.09)
liver	16.28(0.90)	25.28(0.31)	18.61(1.81)	15.14(0.89)
kidney	8.13(1.28)	5.21(0.44)	3.85(0.33)	3.05(0.25)
intestine	3.10(0.61)	7.91(1.05)	12.84(1.18)	21.48(3.17)
spleen	2.57(1.54)	2.31(0.01)	1.76(0.23)	1.52(0.29)
heart	4.87(0.66)	2.66(0.12)	1.67(0.14)	1.28(0.12)
stomach[b]	0.78(0.02)	0.87(0.22)	1.44(0.69)	1.80(0.84)
brain	4.12(0.15)	3.68(0.18)	1.84(0.12)	1.19(0.04)
		[^{125}I]**11**		
blood	1.87(0.18)	1.07(0.08)	1.20(0.15)	1.15(0.16)
liver	15.41(0.98)	21.85(2.14)	15.71(0.96)	12.40(2.38)
kidney	8.33(1.47)	4.31(0.28)	3.40(0.31)	2.32(0.45)
intestine	2.24(0.24)	6.56(0.83)	12.97(1.15)	18.64(2.05)
spleen	2.72(0.20)	1.92(0.33)	1.58(0.31)	1.18(0.17)
heart	5.63(0.80)	2.47(0.14)	1.69(0.06)	1.07(0.17)
stomach[b]	0.73(0.17)	0.63(0.16)	1.17(0.40)	1.06(0.27)
brain	3.22(0.15)	3.61(0.60)	1.89(0.21)	0.99(0.10)
		[^{125}I]**19**		
blood	1.87(0.21)	1.19(0.17)	0.40(0.01)	0.23(0.09)
liver	8.96(1.48)	9.01(0.97)	3.75(0.47)	1.88(0.61)
kidney	7.99(1.08)	6.30(1.02)	4.51(1.59)	1.46(1.12)
intestine	3.52(0.29)	14.39(0.80)	22.51(1.11)	30.05(3.61)
spleen	2.70(0.08)	1.38(0.37)	0.55(0.30)	3.67(5.89)
heart	4.98(0.41)	2.25(0.40)	0.84(0.14)	0.47(0.22)
stomach[b]	0.68(0.06)	0.45(0.18)	0.55(0.33)	0.31(0.07)
brain	4.00(0.18)	2.36(0.33)	0.51(0.07)	0.17(0.05)
		[^{125}I]**20**		
blood	2.77(0.43)	1.58(0.18)	0.66(0.03)	0.20(0.02)
liver	9.77(1.89)	8.24(0.50)	6.80(0.86)	4.78(1.09)
kidney	14.79(2.59)	15.11(2.00)	6.45(0.84)	1.66(0.62)
intestine	3.12(0.37)	11.26(0.63)	22.01(1.34)	27.28(0.48)
spleen	3.92(1.18)	1.55(0.15)	0.56(0.13)	0.17(0.06)
heart	5.51(0.71)	1.60(0.18)	0.53(0.04)	0.12(0.02)
stomach[b]	0.89(0.09)	0.59(0.16)	1.56(0.50)	0.81(0.36)
brain	3.31(0.32)	1.90(0.07)	0.52(0.03)	0.08(0.02)

[a] Expressed as % injected dose per gram. Each value represents the mean (SD in parentheses) for three to five animals at each interval. [b] Expressed as % injected dose per organ.

Conclusions

In conclusion, we successfully designed and synthesized novel radioiodinated flavones as amyloid imaging agents with high in vitro binding affinity for Aβ aggregates. These flavones bound not only amyloid plaques but also NFTs in human AD sections in vitro. In addition, they displayed excellent brain uptake and rapid washout from the brain after injection in normal mice. The combination of high binding affinity for amyloid plaques, high brain uptake, and good clearance in mice of flavone derivatives **10**, **11**, **19**, and **20** provides a series of promising in vivo amyloid imaging agents for SPECT. A more detailed biodistribution study using transgenic mice containing an excess amount of Aβ aggregate deposition in the brain is currently underway. Moreover, additional structural changes on the flavone backbone may lead to more useful amyloid imaging agents for SPECT and PET.

Experimental Sections

All reagents used in syntheses were commercial products and were used without further purification unless otherwise indicated. ^{1}H NMR spectra were obtained on a Varian Gemini 300 spectrometer with TMS as an internal standard. Coupling constants are reported in hertz. The multiplicity is defined by s (singlet), d (doublet), t (triplet), br (broad), and m (multiplet). Mass spectra were obtained on a JEOL IMS-DX instrument.

Chemistry. 4-Nitrobenzoic Acid 2-Acetyl-4-bromophenyl Ester (2). To a stirring solution of 4-nitrobenzoyl chloride (1.00 g, 4.65 mmol) in pyridine (20 mL) in an ice bath was added 5′-bromo-2′-hydroxyacetophenone (863 mg, 4.65 mmol). The reaction mixture was left in the ice bath for 5 min, stirred at room temperature for 30 min, and poured into 1 N aqueous HCl/ice solution with vigorous stirring. The precipitate that formed was filtered and washed with water to yield acetophenone (1.57 g, 92.7% yield). ^{1}H NMR (300 MHz, $CDCl_3$) δ 2.55 (s, 3H), 7.16 (d, J = 8.7 Hz, 1H), 7.76−7.72 (m, 1H), 8.00 (s, 1H), 8.37 (s, 4H). MS *m/z* 365 (MH^+).

1-(5-Bromo-2-hydroxyphenyl)-3-(4-nitrophenyl)propane-1,3-dione (3). A solution of acetophenone **2** (2.31 g, 6.34 mmol) and pyridine (40 mL) was heated to 50 °C, and to it was added pulverized potassium hydroxide (530 mg, 9.45 mmol). The reaction mixture was stirred for 15 min, and when it was cooled, 20 mL of 10% aqueous acetic acid solution was added. The pale-yellow precipitate that formed was filtered to yield **3** (2.01 g, 87.1% yield). ^{1}H NMR (300 MHz, $CDCl_3$) δ 6.83 (s, 2H), 6.95 (d, J = 9.0 Hz, 1H), 7.57 (d, J = 9.0 Hz, 1H), 7.88 (s, 1H), 8.13 (d, J = 9.0 Hz, 2H), 8.36 (d, J = 9.0 Hz, 2H), 11.85 (s, 1H). MS *m/z* 365 (MH^+).

6-Bromo-4′-nitroflavone (4). A mixture of the diketone **3** (2.00 g, 5.49 mmol), concentrated sulfuric acid (0.5 mL), and glacial acetic acid (40 mL) was heated at reflux for 1 h and cooled to room temperature. The mixture was poured onto crushed ice, and the resulting precipitate was filtered to yield **4** (1.79 g, 94.2% yield). MS *m/z* 317 (MH^+).

6-Bromo-4′-aminoflavone (5). A mixture of **4** (100 mg, 0.29 mmol), $SnCl_2$ (275 mg, 1.45 mmol), and EtOH (7 mL) was stirred under reflux for 1 h. After the mixture was cooled to room temperature, 1 M NaOH (50 mL) was added until the mixture became alkaline. After extraction with ethyl acetate (25 mL × 2), the combined organic layers were washed with brine, dried over Na_2SO_4, and evaporated to give 77 mg of **5** (84.3%). ^{1}H NMR (300 MHz, $CDCl_3$) δ 4.15 (s, 2H), 6.70 (s, 1H), 6.72 (d, J = 8.7 Hz, 2H), 7.44 (d, J = 9.0 Hz, 1H), 7.72−7.76 (m, 3H). MS *m/z* 317 (MH^+).

6-Bromo-4′-methylaminoflavone (6). To a mixture of **5** (300 mg, 0.95 mmol) and paraformaldehyde (154 mg, 5.13 mmol) in MeOH (15 mL) was added a solution of NaOMe (28 wt % in MeOH, 0.27 mL) dropwise at 0 °C. The mixture was stirred under reflux for 1 h. After addition of $NaBH_4$ (180 mg, 4.75 mmol), the solution was heated under reflux for 2 h. To the cold mixture 1 M NaOH (30 mL) was added followed by extraction with CH_2Cl_2 (30 mL × 2). The organic phase was dried over Na_2SO_4 and filtered. The solvent was removed, and the residue was purified by silica gel chromatography (3:5 hexane/ethyl acetate) to give 121 mg of **6** (38.6%). ^{1}H NMR (300 MHz, $CDCl_3$) δ 2.91 (s, 3H), 4.18 (s, 1H), 6.62−6.66 (m, 3H), 7.39 (d, J = 8.7 Hz, 1H), 7.69−7.75 (m, 3H), 8.31 (s, 1H).

6-Bromo-4′-dimethylaminoflavone (7). To a stirred mixture of **5** (75 mg, 0.24 mmol) and paraformaldehyde (71 mg, 2.37 mmol) in AcOH (10 mL) was added $NaCNBH_3$ (74.5 mg, 1.19 mmol) in one portion at room temperature. The resulting mixture was stirred at room temperature for 3 h, and 1 M NaOH (50 mL) was added followed by extraction with CH_3Cl (25 × 2 mL). The organic phase was dried over Na_2SO_4. The solvent was removed, and the residue was purified by silica gel chromatography (4:1 hexane/ethyl acetate) to give 70 mg of **7** (85.7%). ^{1}H NMR (300 MHz, $CDCl_3$) δ 3.08 (s, 6H), 6.70−6.77 (m, 3H), 7.43 (d, J = 9.0 Hz, 1H), 7.72−7.82 (m, 3H), 8.34 (s, 1H). MS *m/z* 345 (M^+).

6-(Tributylstannyl)-4′-methylaminoflavone (8). A mixture of **7** (286 mg, 0.87 mmol), bis(tributyltin) (0.55 mL), and $(Ph_3P)Pd$ (41 mg, 0.035 mmol) in a mixed solvent (28 mL, 3:1 dioxane/triethylamine mixture) was stirred at 90 °C for 6 h. The solvent was removed, and the residue was purified by silica gel chromatography (4:1 hexane/ethyl acetate) to give 174 mg of **8** (37.2%). ^{1}H NMR (300 MHz, $CDCl_3$) δ 0.86−1.35 (m, 27H), 2.92 (s, 3H), 4.14 (s, 1H), 7.46 (d, J = 9.0 Hz, 1H), 7.65−7.78 (m, 3H), 8.30 (s, 1H). MS *m/z* 541 (MH^+).

6-(Tributylstannyl)-4′-dimethylaminoflavone (9). The same reaction as described above to prepare **8** was employed, and 54 mg of **9** was obtained in a 16.8% yield from **7**. ^{1}H NMR (300 MHz, $CDCl_3$) δ 0.86−1.56 (m, 27H), 6.72−6.77 (m, 3H), 7.49 (d, J = 9.0 Hz, 1H), 7.71−7.75 (m, 1H), 7.82 (d, J = 9.0 Hz, 2H), 8.30 (s, 1H). MS *m/z* 555 (MH^+).

6-Iodo-4′-methyaminoflavone (10). To a solution of **8** (100 mg, 0.19 mmol) in $CHCl_3$ (20 mL) was added a solution of iodine in $CHCl_3$ (1.5 mL, 1 M) at room temperature. The mixture was stirred at room temperature for 10 min, and $NaHSO_3$ solution (15 mL) was added. The mixture was stirred for 5 min, and the organic phase was separated. The aqueous phase was extracted with CH_3Cl, and the combined organic phase was dried over Na_2SO_4 and filtered. The solvent was removed, and the residue was purified by silica gel chromatography (2:1 hexane/ethyl acetate) to give 20 mg of **10** (28.7%). ^{1}H NMR (300 MHz, $CDCl_3$) δ 2.98 (s, 3H), 4.15 (s, 1H), 6.64−6.69 (m, 3H), 7.28 (d, J = 10.8 Hz, 1H), 7.75 (d, J = 8.4 Hz, 2H), 7.90 (d, J = 9.0 Hz, 1H), 8.53 (s, 1H). MS *m/z* 377 (MH^+). Anal. ($C_{16}H_{12}INO_2$) C, H, N.

6-Iodo-4′-dimethyaminoflavone (11). The same reaction as described above to prepare **10** was used, and 10 mg of **11** was obtained in a 47.3% yield from **9**. ^{1}H NMR (300 MHz, $CDCl_3$) δ 3.09 (s, 6H), 6.71 (d, J = 8.6 Hz, 2H), 6.81 (d, J = 16.3 Hz, 1H), 7.04 (d, J = 16.3 Hz, 1H), 7.21 (d, J = 8.2 Hz, 1H), 7.38 (d, J = 8.2 Hz, 2H), 7.63 (d, J = 8.2 Hz, 2H). MS *m/z* 351 (MH^+). Anal. ($C_{17}H_{14}INO_2$) C, H, N.

4-Methoxybenzoic Acid 2-Acetyl-4-bromophenyl Ester (13). The same reaction as described above to prepare **2** was used, and 3.15 g of **13** was obtained in a 96.5% yield from **12**. ^{1}H NMR (300 MHz, $CDCl_3$) δ 7.72 (d, J = 7.5 Hz, 1H), 8.06 (d, J = 7.2 Hz, 1H), 8.86 (s, 1H), 10.13 (s, 1H).

1-(5-Bromo-2-hydroxyphenyl)-3-(4-methoxyphenyl)-propane-1,3-dione (14). The same reaction as described above to prepare **3** was used, and 1.42 g of **14** was obtained in an 85.2% yield from **13**. ^{1}H NMR (300 MHz, $CDCl_3$) δ 3.90 (s, 3H), 6.68 (s, 2H), 6.90 (d, J = 8.7 Hz, 1H), 7.00 (d, J = 9.3 Hz, 2H), 7.53 (d, J = 9.0 Hz, 1H), 7.83 (s, 1H), 7.94 (d, J = 9.3 Hz, 2H), 12.01 (s, 1H).

6-Bromo-4′-methoxyflavone (15). The same reaction as described above to prepare **4** was used, and 2.01 g of **15** was obtained in a 79.4% yield from **14**. ^{1}H NMR (300 MHz, $CDCl_3$) δ 3.90 (s, 3H), 6.75 (s, 1H), 7.03 (d, J = 9.0 Hz, 2H), 7.45 (d, J = 9.3 Hz, 1H), 7.77 (d, J = 9.0 Hz, 1H), 7.87 (d, J = 9.0 Hz, 2H), 8.35 (s, 1H).

6-Bromo-4′-hydroxyflavone (16). To a solution of **15** (400 mg, 1.21 mmol) in CH_2Cl_2 (215 mL) at 0 °C was added BBr_3 (12 mL, 1 M solution in CH_2Cl_2) dropwise in an ice bath. The mixture was allowed to warm to room temperature and was stirred for 6 h. Water (100 mL) was added while the reaction mixture was cooled in an ice bath to keep the reaction temperature at 0 °C. After extraction with CH_2Cl_2, the combined organic phase was dried over Na_2SO_4. The filtrate was concentrated and the residue was chromatographed on a silica gel column (eluted with 2:5 ethyl acetate/ hexane) to give 50 mg of **16** (13.1%). ^{1}H NMR (300 MHz, $CDCl_3$) δ 6.93−6.96 (m, 3H), 7.76 (d, J = 9.0 Hz, 1H), 7.97−8.00 (m, 3H), 8.09 (s, 1H), 10.38 (s, 1H).

6-(Tributylstannyl)-4′-methoxyflavone (17). The same reaction as described above to prepare **8** was used, and 562 mg of **9** was obtained in a 68.8% yield from **15**. ^{1}H NMR (300 MHz, $CDCl_3$) δ 0.86−1.57 (m, 27H), 3.90 (s, 3H), 6.77 (s, 1H), 7.02−7.05 (m, 2H), 7.56 (m, 1H), 7.68−7.75 (m, 1H), 7.88−7.92 (m, 2H), 8.31 (s, 1H). MS *m/z* 542 (MH^+).

6-(Tributylstannyl)-4′-hydroxyflavone (18). The same reaction as described above to prepare **8** was used, and 36 mg of **18** was obtained in a 43.3% yield from **16**. ^{1}H NMR (300 MHz, $CDCl_3$) δ 0.86−1.59 (m, 27H), 6.31 (s, 1H), 6.77 (s, 1H), 7.00 (d, J = 8.4 Hz, 2H), 7.50−7.55 (m, 1H), 7.85 (d, J = 8.4 Hz, 2H), 8.31 (s, 1H). MS *m/z* 527 (M^+).

6-Iodo-4′-methoxyflavone (19). The same reaction as described above to prepare **10** was used, and 227 mg of **19** was obtained in a 72.2% yield from **17**. ^{1}H NMR (300 MHz, $CDCl_3$) δ 3.90 (s, 3H), 6.75 (s, 1H), 7.03 (d, J = 8.7 Hz, 2H), 7.32 (d, J = 8.7 Hz, 1H), 7.86−7.93 (m, 3H), 8.55 (s, 1H). MS *m/z* 378 (M^+). Anal. ($C_{16}H_{11}IO_3$) C, H.

6-Iodo-4′-hydroxyflavone (20). The same reaction as described above to prepare **16** was used, and 79 mg of **20** was obtained in a 44.3% yield from **19**. ^{1}H NMR (300 MHz, $CDCl_3$) δ 6.93−6.95 (m, 3H), 7.61 (d, J = 8.7 Hz, 1H), 7.98 (d, J = 8.4 Hz, 2H), 8.28−8.30 (m, 1H), 8.27 (s, 1H), 10.37 (s, 1H). MS *m/z* 364 (M^+). Anal. ($C_{15}H_9IO_3$) C, H.

Iododestannylation Reaction. The radioiodinated forms of compounds **10**, **11**, **19**, and **20** were prepared from the corresponding tributyltin derivatives by an iododestannylation. Briefly, to initiate the reaction, 50 μL of H_2O_2 (3%) was added to a mixture of a tributyltin derivative (100 μg/50 μL EtOH), 1.5 mCi sodium [^{125}I]iodide (specific activity 2200 Ci/mmol), and 100 μL of 1 N HCl in a sealed vial. The reaction was allowed to proceed at room temperature for 10 min and terminated by addition of $NaHSO_3$. The reaction, after neutralization with sodium bicarbonate, was extracted with ethyl acetate. The extract was dried by passing through an anhydrous Na_2SO_4 column and was then blown to dryness with a stream of nitrogen gas. The radioiodinated ligand was purified by HPLC on a Cosmosil C18 column with an isocratic solvent of H_2O/acetonitrile (2/3) at a flow rate of 1.0 mL/min. The purified ligand was stored at −20 °C for in vitro binding and biodistribution studies.

Binding Assays Using the Aggregated A*β* Peptide in Solution. A solid form of Aβ(1−40) and Aβ(1−42) was purchased from Peptide Institute (Osaka, Japan). Aggregation of peptides was carried out by gently dissolving the peptide (0.5 mg/mL) in a buffer solution (pH 7.4) containing 10 mM sodium phosphate and 1 mM EDTA. The solutions were incubated at 37 °C for 36−42 h with gentle and constant shaking. Binding studies were carried out in 12 mm × 75 mm borosilicate glass tubes according to the procedure described before[16] with some modification. For saturation studies, a solution of [^{125}I]**11** (final concentration, 0.78−100 nM) was prepared by mixing nonradioactive **11**. Nonspecific binding was defined in the presence of 100 nM nonradioactive **11**. For inhibition studies, 1 mL of the reaction mixture contained 50 μL of inhibitors (10^{-5}−10^{-10} M in 10% EtOH) and 0.05 nM of radiotracer in 10% EtOH. The binding assay was performed by mixing 50 μL of Aβ(1−40) or Aβ(1−42) aggregates (57 nM in the final assay mixture), an appropriate concentration of 50 μL of [^{125}I]**11**, and 900 μL of 10% ethanol. After incubation for 3 h at room temperature, the binding mixture was filtered through GF/B filters (Whatman, Kent, U.K.) using an M-24 cell harvester (Brandel, Gaithersburg, MD). Filters containing the bound ^{125}I ligand were counted in a γ camera counter. The dissociation constant (K_d) of compound **11** was determined by Scatchard analysis using GraphPad Prism (GraphPad Software, San Diego, CA). For inhibition studies, a mixture containing 50 μL of test compounds (8 pM to 12.5 μM in 10% ethanol), 50 μL of 0.02 nM [^{125}I]**11**, 50 μL of Aβ(1−40) or Aβ-(1−42) aggregates, and 850 μL of 10% ethanol was incubated at room temperature for 3 h. The mixture was then filtered through Whatman GF/B filters using a Brandel M-24 cell harvester, and the filters containing the bound ^{125}I ligand were counted in a γ counter. Values for the half-maximal inhibitory concentration (IC_{50}) were determined from displacement curves of three independent experiments using GraphPad Prism, and those for the inhibition constant (K_i) were calculated using the Cheng−Prusoff equation:[27] $K_i = IC_{50}/(1 + [L]/K_d)$, where [L] is the concentration of [^{125}I]**11** used in the assay, and K_d is the dissociation constant of compound **11**.

Partition Coefficient Determination. Partition coefficients were measured by mixing the radioiodinated tracers with 3 mL each of 1-octanol and buffer (0.1 M phosphate, pH 7.4) in a test tube. The test tube was vortexed for 3 min at room temperature, followed by centrifugation for 5 min. Two weighed samples (0.5 mL each) from the 1-octanol and buffer layers were counted in a well counter. The partition coefficient was determined by calculating the ratio of cpm/0.5 mL of the 1-octanol to that of buffer. A sample from the octanol layer was repartitioned with the same volume of buffer until

consistent partitions coefficient values were obtained. The measurement was done in triplicate and repeated three times.

Staining of Senile Plaques in Human AD Brain Sections. Post-mortem brain tissues from AD cases (74−79 years old) were confirmed by conventional neuropathology, including amyloid and τ staining in addition to silver staining. Experiments were performed under the regulations of the ethics committee of Osaka City University Medical School. Five-micrometer-thick serial sections of paraffin-embedded blocks from the temporal cortex were used for staining. Paraffin sections were first taken through five 10-min incubations in xylene and five 10-min incubations in 100% EtOH to completely deparaffinize them, followed by two 5-min washes in water and then PBS. Tissue sections were immersed in the compound solution at various concentrations. At greater than 0.5 mM concentration, we used 50% EtOH in PBS to ensure the full solubilization of the compound. Finally, the sections were washed in PBS for 15 min. Thereafter, the sections were incubated in EtOH and xylene and embedded in Entellan Neu (Merck, Darmstadt, Germany). Fluorescent sections were viewed using a BX50 fluoromicroscope with a M-3204C CCD camera (Olympus, Tokyo) equipped with a G-filter/rhodamine. The sections were also immunostained with DAB as a chromogen using monoclonal antibodies against Aβ[28] and tau[29] as previously described.

In Vivo Biodistribution in Normal Mice. Animal studies were conducted in accordance with our institutional guidelines and were approved by Nagasaki University Animal Care Committee. A saline solution (100 μL) containing radiolabeled agents (2 μCi) was injected directly into the tail vein of ddY mice (5 weeks old, average weight of 25−30 g). The mice were sacrificed at various time points postinjection. The organs of interest were removed and weighed, and the radioactivity was counted with an automatic γ counter (Aloka 3000).

Acknowledgment. The authors thank Drs. Mei-Ping Kung and Hank F. Kung (University of Pennsylvania) for helpful discussions. This work was supported in part by a Grant-in-Aid for Young Scientists (B) (Grant No. 16790734) and Scientific Research (B) (Grant No. 15390014) from the Ministry of Education, Culture, Sports, Science and Technology, Japan.

Note Added after ASAP Publication. This manuscript was released ASAP on October 19, 2005, with errors in the caption for Figure 4. The correct version was posted on October 27, 2005.

References

(1) Selkoe, D. J. Alzheimer's disease: genes, proteins, and therapy. *Physiol. Rev.* **2001**, *81*, 741−766.
(2) Selkoe, D. J. Imaging Alzheimer's amyloid. *Nat. Biotechnol.* **2000**, *18*, 823−824.
(3) Mathis, C. A.; Wang, Y.; Klunk, W. E. Imaging beta-amyloid plaques and neurofibrillary tangles in the aging human brain. *Curr. Pharm. Des.* **2004**, *10*, 1469−1492.
(4) Nordberg, A. PET imaging of amyloid in Alzheimer's disease. *Lancet Neurol.* **2004**, *3*, 519−527.
(5) Ono, M.; Wilson, A.; Nobrega, J.; Westaway, D.; Verhoeff, P.; et al. ^{11}C-labeled stilbene derivatives as Abeta-aggregate-specific PET imaging agents for Alzheimer's disease. *Nucl. Med. Biol.* **2003**, *30*, 565−571.
(6) Mathis, C. A.; Wang, Y.; Holt, D. P.; Huang, G. F.; Debnath, M. L.; et al. Synthesis and evaluation of ^{11}C-labeled 6-substituted 2-arylbenzothiazoles as amyloid imaging agents. *J. Med. Chem.* **2003**, *46*, 2740−2754.
(7) Agdeppa, E. D.; Kepe, V.; Liu, J.; Flores-Torres, S.; Satyamurthy, N.; et al. Binding characteristics of radiofluorinated 6-dialkylamino-2-naphthylethylidene derivatives as positron emission tomography imaging probes for beta-amyloid plaques in Alzheimer's disease. *J. Neurosci.* **2001**, *21*, RC189.
(8) Verhoeff, N. P.; Wilson, A. A.; Takeshita, S.; Trop, L.; Hussey, D.; et al. In-vivo imaging of Alzheimer disease beta-amyloid with [^{11}C]SB-13 PET. *Am. J. Geriatr. Psychiatry* **2004**, *12*, 584−595.
(9) Klunk, W. E.; Engler, H.; Nordberg, A.; Wang, Y.; Blomqvist, G.; et al. Imaging brain amyloid in Alzheimer's disease with Pittsburgh compound-B. *Ann. Neurol.* **2004**, *55*, 306−319.
(10) Shoghi-Jadid, K.; Small, G. W.; Agdeppa, E. D.; Kepe, V.; Ercoli, L. M.; et al. Localization of neurofibrillary tangles and beta-amyloid plaques in the brains of living patients with Alzheimer disease. *Am. J. Geriatr. Psychiatry* **2002**, *10*, 24−35.
(11) Kung, M. P.; Hou, C.; Zhuang, Z. P.; Zhang, B.; Skovronsky, D.; et al. IMPY: an improved thioflavin-T derivative for in vivo labeling of beta-amyloid plaques. *Brain Res.* **2002**, *956*, 202−210.
(12) Zhuang, Z. P.; Kung, M. P.; Wilson, A.; Lee, C. W.; Plossl, K.; et al. Structure−activity relationship of imidazo[1,2-*a*]pyridines as ligands for detecting β-amyloid plaques in the brain. *J. Med. Chem.* **2003**, *46*, 237−243.
(13) Kung, M. P.; Hou, C.; Zhuang, Z. P.; Cross, A. J.; Maier, D. L.; et al. Characterization of IMPY as a potential imaging agent for beta-amyloid plaques in double transgenic PSAPP mice. *Eur. J. Nucl. Med. Mol. Imaging* **2004**, *31*, 1136−1145.
(14) Wang, Y.; Klunk, W. E.; Huang, G. F.; Debnath, M. L.; Holt, D. P.; et al. Synthesis and evaluation of 2-(3′-iodo-4′-aminophenyl)-6-hydroxybenzothiazole for in vivo quantitation of amyloid deposits in Alzheimer's disease. *J. Mol. Neurosci.* **2002**, *19*, 11−16.
(15) Ono, K.; Yoshiike, Y.; Takashima, A.; Hasegawa, K.; Naiki, H.; et al. Potent anti-amyloidogenic and fibril-destabilizing effects of polyphenols in vitro: implications for the prevention and therapeutics of Alzheimer's disease. *J. Neurochem.* **2003**, *87*, 172−181.
(16) Zhuang, Z. P.; Kung, M. P.; Hou, C.; Skovronsky, D. M.; Gur, T. L.; et al. Radioiodinated styrylbenzenes and thioflavins as probes for amyloid aggregates. *J. Med. Chem.* **2001**, *44*, 1905−1914.
(17) Zhuang, Z. P.; Kung, M. P.; Hou, C.; Plossl, K.; Skovronsky, D.; et al. IBOX(2-(4′-dimethylaminophenyl)-6-iodobenzoxazole): a ligand for imaging amyloid plaques in the brain. *Nucl. Med. Biol.* **2001**, *28*, 887−894.
(18) Kung, H. F.; Lee, C. W.; Zhuang, Z. P.; Kung, M. P.; Hou, C.; et al. Novel stilbenes as probes for amyloid plaques. *J Am Chem Soc* **2001**, *123*, 12740−12741.
(19) Ono, M.; Kung, M. P.; Hou, C.; Kung, H. F. Benzofuran derivatives as Abeta-aggregate-specific imaging agents for Alzheimer's disease. *Nucl. Med. Biol.* **2002**, *29*, 633−642.
(20) Ares, J. J.; Outt, P. E.; Randall, J. L.; Murray, P. D.; Weisshaar, P. S.; et al. Synthesis and biological evaluation of substituted flavones as gastroprotective agents. *J. Med. Chem.* **1995**, *38*, 4937−4943.
(21) Barluenga, A. M.; Bayron, G.; Asensio, A. A new and specific method for the monomethylation of primary amine. *J. Chem. Soc., Chem. Commun.* **1984**, 1334−1335.
(22) Espeseth, A. S.; Xu, M.; Huang, Q.; Coburn, C. A.; Jones, K. L.; et al. Compounds that bind APP and inhibit Abeta processing in vitro suggest a novel approach to Alzheimer disease therapeutics. *J. Biol. Chem.* **2005**, *280*, 17792−17797.
(23) Iwatsubo, T.; Odaka, A.; Suzuki, N.; Mizusawa, H.; Nukina, N.; et al. Visualization of A beta 42(43) and A beta 40 in senile plaques with end-specific A beta monoclonals: evidence that an initially deposited species is A beta 42(43). *Neuron* **1994**, *13*, 45−53.
(24) Morris, J. C.; Storandt, M.; McKeel, D. W., Jr.; Rubin, E. H.; Price, J. L.; et al. Cerebral amyloid deposition and diffuse plaques in "normal" aging: Evidence for presymptomatic and very mild Alzheimer's disease. *Neurology* **1996**, *46*, 707−719.
(25) Price, J. L.; Morris, J. C. Tangles and plaques in nondemented aging and "preclinical" Alzheimer's disease. *Ann. Neurol.* **1999**, *45*, 358−368.
(26) Dishino, D. D.; Welch, M. J.; Kilbourn, M. R.; Raichle, M. E. Relationship between lipophilicity and brain extraction of C-11-labeled radiopharmaceuticals. *J. Nucl. Med.* **1983**, *24*, 1030−1038.
(27) Cheng, Y.; Prusoff, W. H. Relationship between the inhibition constant (K1) and the concentration of inhibitor which causes 50% inhibition (I50) of an enzymatic reaction. *Biochem. Pharmacol.* **1973**, *22*, 3099−3108.
(28) Mori, H.; Takio, K.; Ogawara, M.; Selkoe, D. J. Mass spectrometry of purified amyloid beta protein in Alzheimer's disease. *J. Biol. Chem.* **1992**, *267*, 17082−17086.
(29) Endoh, R.; Ogawara, M.; Iwatsubo, T.; Nakano, I.; Mori, H. Lack of the carboxyl terminal sequence of tau in ghost tangles of Alzheimer's disease. *Brain Res.* **1993**, *601*, 164−172.

JM050635E